THE JOURNAL OF PHYSICAL CHEMISTRY C

Article

pubs.acs.org/JPCC

Growth of Competing Crystal Phases of α-Sexithiophene Studied by Real-Time *in Situ* X-ray Scattering

C. Lorch, R. Banerjee, C. Frank, J. Dieterle, A. Hinderhofer, A. Gerlach, and F. Schreiber*

Insitut für Angewandte Physik, Universität Tübingen, Auf der Morgenstelle 10, 72076 Tübingen, Germany

ABSTRACT: We report on a real-time *in situ* study of the growth of α-sexithiophene on silicon oxide substrates. Synchrotron-based X-ray diffraction experiments were performed during and directly after the growth in order to monitor the growth process. We observed a coexistence of two different crystal phases for different substrate temperatures. For films prepared at 233 and 308 K a disordered phase (β-phase) seems to be dominant compared to films prepared at 373 K where the so-called low-temperature bulk crystal phase (LT-phase) is dominant. From real-time measurements during growth we observed a temperature and film thickness dependent effect on the fraction of both phases in one sample. At 373 K the film growth begins primarily in the β-phase, and above a certain thickness the film growth proceeds mainly in the LT-phase. However, at 308 K the film growth is dominated by the β-phase for the entire thickness. We show that for kinetically limited growth conditions (high deposition rate and/or low substrate temperature) substrate induced growth effects are dominant.

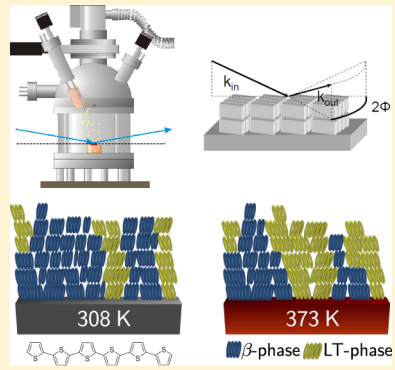

INTRODUCTION

Organic electronics are an attractive alternative to common inorganic devices, *inter alia* due to potentially low preparation costs, low-temperature processing, and the possibility of using flexible substrates.[1−7] Organic semiconductors (OSCs) are also used as active layers in organic light-emitting diodes, organic photovoltaics (OPV), and organic field effect transistors (OFETs). For small molecule OSCs, the crystallinity of the thin films and the relative orientation of the individual molecules constituting the thin film are crucially important for the efficiencies of such devices. Oligothiophenes are an important class of OSC materials. In particular, α-sexithiophene (6T) (Figure 1a) is considered very promising. 6T has shown a high open circuit voltage in combination with diindenoperylene in OPV cells[8] and high hole mobility of up to 4×10^{-2} cm^2 V^{-1} s^{-1} in OFETs.[9] As in many other small molecule OSCs, the crystal structure and the crystal defect density are crucial for the performance.[10−12] In this study we focus on the growth and structure of 6T on native silicon oxide (nSi).

In general, depending on the substrate, the preparation conditions and the sample state (i.e., thin film or single crystal), there are several phases of 6T with different crystal structures reported.[13−16] In thin films on substrates with low interaction energies, mostly the so-called low-temperature phase (LT-phase) of single crystals, reported by Horowitz et al.,[16] and the thin film β-phase[14,15] are found. Figure 1b depicts the unit cell of the LT crystal phase. For 6T on SiO_2 several studies of growth, structure, and charge transport report that 6T molecules are oriented mostly perpendicularly to the substrate.[14,15,17−21] Different anisotropic growth scenarios on fused silica and stretched polyethylene substrates were measured via absorption spectroscopy by Oelkrug et al.[22] On TiO_2 the formation of domains of the LT-phase[16] was observed.[23,24] Highly ordered pyrolytic graphite (HOPG), mica, and KCl have also been used as substrates for the growth of 6T.[25−29] The adsorption of 6T on single crystal Cu surfaces was studied by scanning tunneling microscopy, X-ray photo-

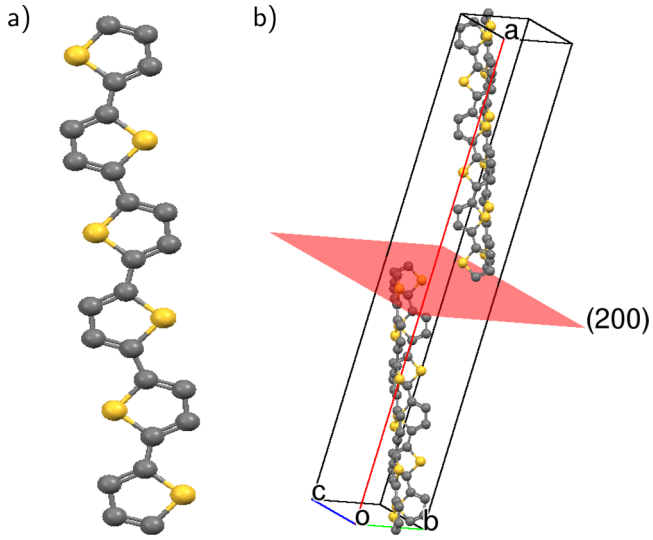

Figure 1. (a) Structure formula of a single α-6T molecule. (b) Crystal unit cell of the LT-phase[16] together with the (200) plane, responsible for the main reflections in the standing-up configuration of the molecules. *o* corresponds to the origin of the unit cell, and *a*, *b*, and *c* indicate the directions of unit cell vectors. The lattice parameters of the depicted crystal structure are $a = 44.708(6)$ Å, $b = 7.851(3)$ Å, $c = 6.029(2)$ Å, $\alpha = 90°$, $\beta = 90.76(2)°$, and $\gamma = 90°$.[16]

Received: October 13, 2014
Revised: December 8, 2014
Published: December 8, 2014

DOI: 10.1021/jp510321k
J. Phys. Chem. C 2015, 119, 819−825

electron spectroscopy, and near-edge X-ray absorption fine structure[30] as well as X-ray diffraction[31] revealing mainly lying 6T domains following closely the substrate lattice. On metal single crystal substrates the molecular orientations and adsorption structures of 6T have also been studied.[32−35] Furthermore, 6T was used as a templating layer for the growth of *p*-sexiphenyl and vice versa, leading in both cases to an epitaxial relationship between the two organic compounds.[36−38]

Films prepared on thermally oxidized silicon wafers (SiO_x) are particularly interesting for applications like OFETs and also for hybrid inorganic−organic devices. For relatively thick 6T films (100 nm) deposited on thermally oxidized silicon wafers it has been reported that 6T arranges in different phases for various substrate temperatures at moderate deposition rates (6−30 nm/min).[15] It has also been demonstrated that the deposition rate has a huge impact on the resulting crystal phase.[19] For relatively low deposition rates, the molecules adopt a thermodynamically favorable packing (LT-phase), whereas at higher rates (about 36−48 nm/min) the films crystallize predominantly in a phase similar to a frozen smectic state (β-phase).[19]

In the present study, we used different substrate temperatures to prepare thin films comprising the β-phase and the LT-phase. Our time-resolved (and hence film thickness dependent) measurements provide important insights into the evolution and competition of the different crystalline phases of 6T and their dependence on the preparation conditions. Since the growth of organic thin films is in general not in equilibrium, it is imperative to employ real-time measurements to investigate the growth kinetics.[39−42] The real-time investigations are necessary to observe possible effects of transient crystal phases. Furthermore, we can follow the evolution and competition of different structural features which is not possible postgrowth.

EXPERIMENTAL SECTION

6T was purchased from Sigma-Aldrich and purified twice by temperature gradient sublimation before use. The samples were prepared and measured in a portable ultrahigh vacuum chamber.[43] Before the installation of the silicon substrates with a native oxide layer of approximately 1.8 nm, they were cleaned in an ultrasonic bath with acetone, isopropanol, and purified water. Before each sample preparation the substrates were heated up to 770 K. The base pressure of the vacuum system was below 10^{-9} mbar, increasing to approximately 3×10^{-9} mbar during the evaporation of 6T. The evaporation rate, monitored with a water-cooled quartz crystal microbalance, which was calibrated via X-ray reflectivity (XRR), varied between 0.13 and 0.16 nm/min. For all films the nominal thickness was 20 nm. The substrate temperature during growth was 233, 308, or 373 K. The temperature was stabilized via a combination of resistive heating and liquid nitrogen cooling. All experiments were performed at the MS-X04SA/Surface Diffraction beamline at the Swiss Light Source (SLS)[44] using an energy of 12.4 keV (corresponding to a wavelength of 0.999 Å) and a PILATUS II area detector. Slits placed directly in front of the detector were used to mimic a point detector. For the samples prepared at 308 and 373 K the growth was followed with real-time grazing incidence X-ray diffraction (GIXD) measurements. The scan range of the in-plane scattering angle 2θ was 11°−16°, which corresponds to an in-plane momentum transfer q_{xy} = 1.205−1.749 $Å^{-1}$. The critical angle of the 6T/Si system is α_c = 0.14°, and the incidence angle for the measurements was set to α_{in} = 0.13°. The time difference between the start of two successive scans was 6 min, which leads to a 1 nm "thickness" (i.e., submonolayer) resolution for the growth at a deposition rate of 0.16 nm/min.

RESULTS AND DISCUSSION

X-ray Reflectivity. XRR is used to obtain information about the film structure in a direction perpendicular to the surface of the film.[45] Figure 2 depicts the measured XRR data of

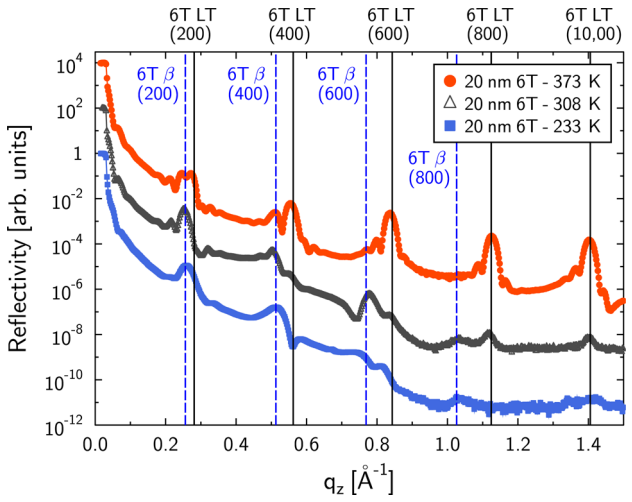

Figure 2. XRR measurements of 6T grown at different substrate temperatures. For 373 K (red solid dots) one can identify several orders of the Bragg reflections corresponding to the 6T LT bulk crystalline phase (positions marked with black vertical lines). In the films prepared at 308 K (black triangles) and 233 K (blue squares) the observed Bragg peaks can be mainly allocated to the β-phase (Bragg positions corresponding to domains of upright standing molecules are marked with blue dashed lines).

the different samples. For all the films the Kiessig oscillations in the low q_z range beyond the total reflection edge are not very pronounced. This is a strong indication that the top surfaces of the films are relatively rough.

In the plot, corresponding to the sample prepared at 373 K (filled red circles in Figure 2), Bragg peaks up to an out-of-plane momentum transfer $q_z \approx 1.4$ $Å^{-1}$ are visible. This is an indicator that this sample exhibits a high out-of-plane crystalline order. The Bragg peaks marked with vertical black solid lines are due to reflections from crystallites with a lattice spacing of d = 44.73 Å. These crystallites can be identified as the almost upright standing molecules in the LT-phase (d = 44.708 Å).[16] The fringes around the Bragg reflections ("Laue oscillations") correspond to the coherent out-of-plane crystallite size ($D_{coh\perp}$), calculated from the periodicity of the oscillations (Δq_z) by $D_{coh\perp} = 2\pi/\Delta q_z$. For the LT-phase crystallites in the 373 K film one obtains $D_{coh\perp} = 23 \pm 3$ nm. Comparing this to the nominal film thickness of 20 nm leads to the conjecture that crystallites are formed with a size similar to the total film thickness, in a continuous columnar growth from the substrate to the top of the film. Weak Bragg reflections are observed at q_z = 0.248 and 0.513 $Å^{-1}$ for the sample prepared at 373 K. These reflections correspond to crystallites of the β-phase.

In the XRR data of the film prepared at 308 K (black open triangles in Figure 2) the Bragg reflections of the standing LT-phase are weak with no Laue oscillations, implying that the out-of-plane coherent crystallite size of the LT-phase is rather small. However, Bragg reflections of the β-phase are observed very

DOI: 10.1021/jp510321k
J. Phys. Chem. C 2015, 119, 819−825

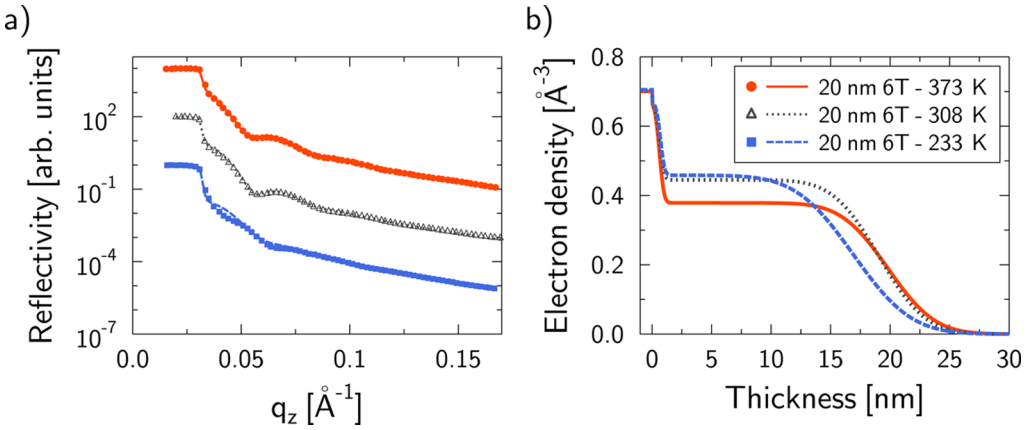

Figure 3. (a) Experimental XRR data (symbols) and the simulated values using a one-box-model (lines) up to q_z = 0.171 Å^{-1} for three growth temperatures are shown. (b) Corresponding electron density profiles extracted from the fits.

Table 1. Summary of the Films Deposited at Different Temperature with Thickness d, Roughness σ, Thickness-to-Roughness Ratio d/σ, Electron Densities ρ_e (at a Thickness of 5 nm) Extracted from the Electron Density Profiles from the XRR Fits, and Coherent Out-of-Plane Crystallite Size $D_{coh\perp}$ Values Calculated from Laue Oscillations

substrate temp (K)	thickness d [nm]	roughness σ [nm]	d/σ	electron density ρ_e [Å^{-3}]	$D_{coh\perp}$ [nm]
373	19.2 ± 0.2	3.1 ± 0.2	6.2 ± 0.4	0.38 ± 0.02	23.1 ± 3.1
308	18.5 ± 0.4	3.1 ± 0.1	6.0 ± 0.5	0.45 ± 0.02	17.4 ± 2.3
233	16.2 ± 0.9	3.8 ± 0.3	4.3 ± 1.2	0.46 ± 0.02	

close to the q_z values expected from the literature.[15,19] The fringes close to the (200) Bragg reflection of the β-phase correspond to an out-of-plane coherent crystalline size of $D_{coh\perp}$ = 17 ± 2 nm.

For the film prepared at 233 K (filled blue squares in Figure 2) no peaks having their origin in the standing-up phase of the LT-phase are observed. The first and second order of the β-phase (h00) reflections are seen at q_z = 0.256 Å^{-1} and q_z = 0.513 Å^{-1}, respectively. Presumably, the out-of-plane coherent length of the crystallites causing these reflections is rather small, and therefore no Laue oscillations are observable.

The XRR data were fitted with the Parratt formalism[46] using the GenX-software.[47] Since the texture of the films consists of various crystalline phases, a model was used where the entire film is described by only one box having a certain thickness, surface roughness, and electron density. The data were fitted in the range q_z = 0−0.171 Å^{-1} in order to extract the film thickness and the roughness of the films (Figure 3a). These are given in Table 1. Comparing the resulting film thickness d with the roughness σ, one can see that for the film prepared at 233 K the ratio d/σ = 4.3 of film thickness to roughness is significantly smaller compared to 308 and 373 K (d/σ = 6.0 and d/σ = 6.2, respectively). For amorphously growing organic compounds one would expect a higher roughness for high temperature films,[48] and usually the crystallinity of thin organic films improves with increasing substrate temperature.[49,50] That this correlation is not observed here can be attributed to the fact that at different substrate temperatures the dominant crystalline phase varies between the LT-phase and the β-phase or a mixture of both phases of 6T.

Figure 3b shows the extracted electron densities for the different samples (Table 1). The fitted values (0.38, 0.45, and 0.46 Å^{-3} for 373, 308, and 233 K, respectively) are all lower than the values obtained by calculations using the unit cell volume (0.48 and 0.46 1/Å^3 for the LT-phase and the β-phase, respectively). This leads to the assumption that the thin films do not form perfectly filled layers, meaning that the packing fraction is below one. Furthermore, the electron density increases for lower substrate temperatures, showing that also the substrate temperature influences the packing fraction.

Grazing Incidence Diffraction. The in-plane crystalline structure of the samples was investigated via GIXD measurements.[45] The GIXD data of the films prepared are shown in Figure 4. For the film with a substrate temperature of 373 K, the peaks corresponding to the standing-up 6T LT-phase are prominent. The peak at q_{xy} = 1.38 Å^{-1} can be associated with the β-phase.[19] For the sample prepared at 308 K all peaks can

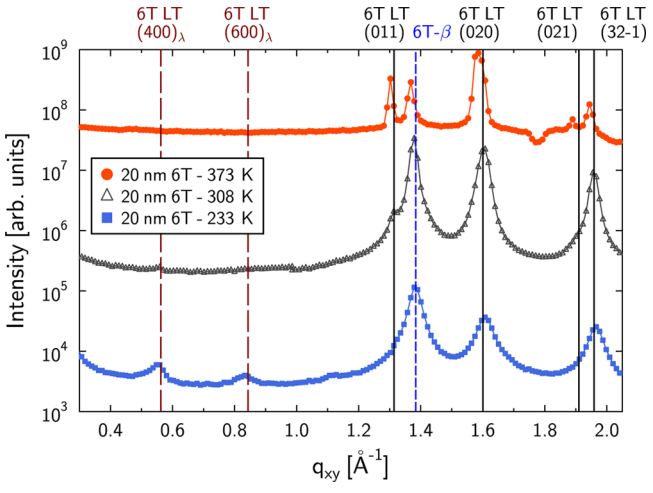

Figure 4. GIXD measurements of 6T grown at different substrate temperatures at an incident angle of α_{in} = 0.13°. For the films prepared at 233 K (blue squares) and 308 K (black triangles) the peak corresponding to the β-phase is the dominant one (marked with a blue dashed line). At 233 K weak reflections from lying crystal domains are observed (vertical brown dashed lines and marked with λ). For the film prepared at 373 K the LT-phase Bragg peaks are dominant.

DOI: 10.1021/jp510321k
J. Phys. Chem. C 2015, 119, 819−825

be associated with standing-up 6T molecules corresponding to the β-phase or the LT-phase with similar intensities.

In the data of the film prepared at 233 K the β-phase peak is again the one with the highest intensity. The (011) LT peak is not observed. Furthermore, the intensities of the (020) and (021) LT peaks are weaker than the corresponding ones in the other films. Additionally, small peaks at lower q_{xy} values (q_{xy} = 0.55 and 0.82 Å^{-1}) are detected. These peaks correspond to domains of lying 6T molecules (LT-phase) with a small coherent size. On comparison of the films at the three different temperatures, a slight shift of almost all peaks toward lower q_{xy} values with increasing temperature is observed. This shift corresponds to a change in the in-plane lattice parameter by approximately 1%. This can be attributed to a small change in the orientation, e.g., a slightly different tilt angle, of the molecules due to different diffusion energies of the molecules at different substrate temperatures or due to different interaction potentials of the surrounding molecules, oriented in different crystal phases. However, using the given experimental setup and resolution, it is not possible to quantitatively estimate any systematic variation.

The observed peaks of the films were fitted, and the Scherrer formula[51] $D_{cohll} = 2\pi K/\text{fwhm}$ was used to calculate the in-plane coherent crystallite size (D_{cohll}). Here, K = 0.94 is Scherrer's constant for spherically shaped grains, and fwhm is the full width at half-maximum of the fitted peaks. Since no instrumental line broadening was taken into account, the reported values are only lower limits but all are well below the resolution limit of the in-plane experiments $\Delta D_{cohll} \approx 100$ nm. D_{cohll} values for all samples are summarized in Table 2.

Table 2. Summary of the In-Plane Coherent Crystallite Sizes

	lower limit of coherent crystallite size D_{cohll} [nm]			
	LT-phase			
substrate temp (K)	(011)	(020)	(32−1)	β-phase
373	50.1	20.1	29.8	30.7
308	21.7	17.0	22.0	26.1
233		11.0	11.5	15.3

There is a significant difference in the in-plane coherent crystallite sizes between the films prepared at 233 and 373 K. D_{cohll} of the LT-phase domains increases from 11.0 to 20.1 nm and from 11.5 to 29.8 nm for the (020) and (32−1) peak, respectively. For the β-phase domains an increase from 15.3 to 30.7 nm is observed. Hence, this increase by a factor of approximately 2 is independent of the crystal phase and seems to depend merely on the change in the preparation conditions (here the substrate temperature).

Figure 5 depicts 2D reciprocal space maps of the three different films in a q_{xy} range of 1.2−1.7 Å^{-1}. One can clearly recognize the Bragg reflections related to the β-phase and the (020) peak of the LT crystal phase. The peak corresponding to the β-phase is very broad in q_z direction, indicating a small out-of-plane coherent crystallite size.

Real-Time Grazing Incidence Diffraction. During the growth of the samples prepared at 308 and 373 K real-time GIXD scans, monitoring the evolution of the β peak (q_{xy} = 1.38 Å^{-1}) and of the (020) LT-phase peak (q_{xy} = 1.60 Å^{-1}) were performed.[52−55] With these measurements we are able to follow and understand the competition between different crystal phases. This is necessary since conventional GIXD

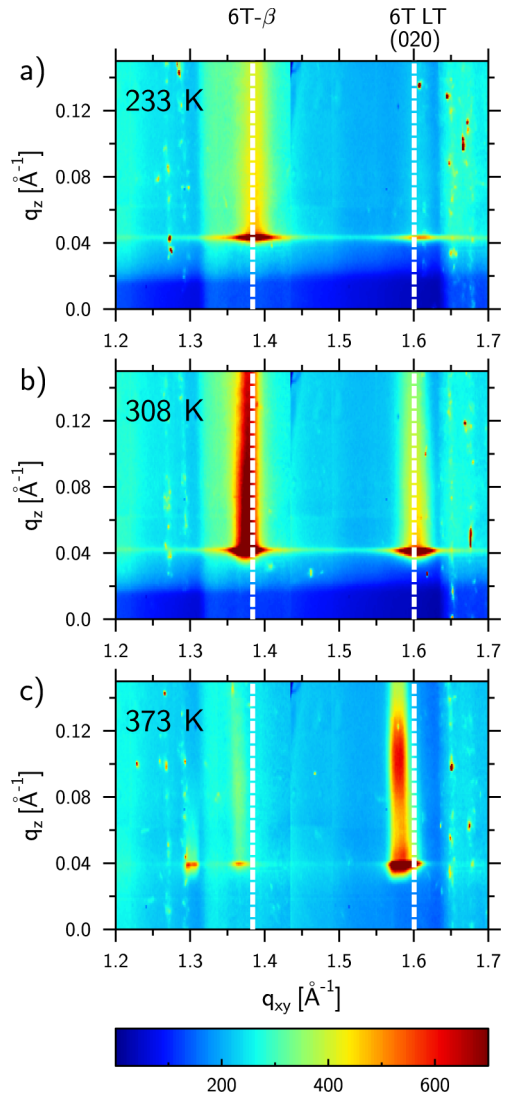

Figure 5. 2D reciprocal space maps at (a) 233, (b) 308, and (c) 373 K. The images are a combination of two pictures (first one covers a q_{xy} range of 1.2−1.44 Å^{-1} and the second one covers a q_{xy} range of 1.44−1.7 Å^{-1}) and were taken at an incident angle of α_{in} = 0.13°. The white dashed lines mark the positions of the reflections arising from the β-phase (q_{xy} = 1.38 Å^{-1}) and the LT-phase (q_{xy} = 1.60 Å^{-1}). In the films prepared at 233 and 308 K, the reflection corresponding to the β-phase is broadened and extended in q_z, indicating a relatively small out-of-plane coherent crystallite size.

measurements mostly probe the structure of the entire organic film (apart from penetration depth effects) and hence do not provide time-resolved information. The peaks were fitted using pseudo-Voigt functions. The shape of the peaks (i.e., the full width at half-maximum and the mixing coefficient for the pseudo-Voigt function) did not vary significantly during the film growth. Hence, D_{cohll} does not significantly increase during the growth under the conditions employed. However, the amount of material forming the specific domains increases as the growth progresses. Figure 6 depicts the evolution of the peak intensity (the area under the fitted curves) of the β-phase and of the LT-phase peak vs the film thickness. The signals were normalized to the value of the highest peak at the end of the growth. We note that the x-axes show slightly different ranges due to different film thicknesses extracted from the fitted XRR data. For the sample prepared at 308 K the formation of

DOI: 10.1021/jp510321k
J. Phys. Chem. C 2015, 119, 819−825

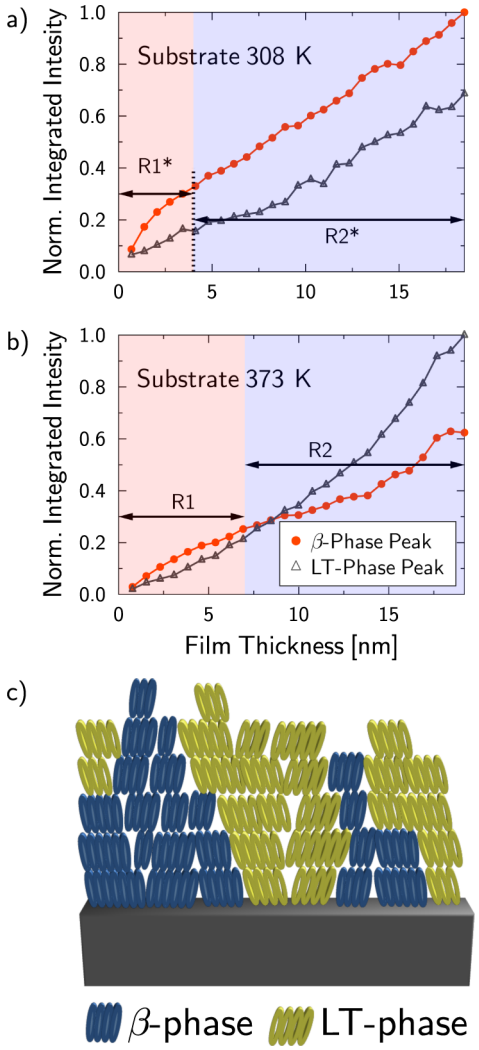

Figure 6. Peak intensity evolution of the β-phase (q_{xy} = 1.38 Å^{-1}) and LT-phase (q_{xy} = 1.60 Å^{-1}) during growth of 6T films prepared at (a) 308 and (b) 373 K substrate temperature, respectively. For 373 K the β-phase dominates for the first 8 nm. Above this thickness the LT-phase is the dominating crystal phase. However, for 308 K the β-phase is predominant during the entire film growth. (c) Sketch of the film growth behavior at 373 K. At the beginning the β-phase is dominant, but above a certain thickness the LT-phase grows predominantly at the expense of the β-phase.

domains belonging to the β-phase is faster than the one of domains of the LT-phase up to a film thickness of approximately 4 nm (region marked with R1* in Figure 6a). Beyond this thickness (region R2*) the intensities of both phases grow simultaneously and linearly with film thickness, with the β-phase being slightly faster than the LT-phase.

For the sample grown at a substrate temperature of 373 K (Figure 6b) the growth of β-phase domains is faster than the one of LT-phase domains only for low film thicknesses up to 7 nm (region R1). Furthermore, the intensity of the peak corresponding to the LT-phase increases nonlinearly in region R1. In the thickness range from 7 to 19.2 nm (region R2) the intensity increase of the β-phase is significantly slower than for the LT-phase. The peak intensity of the LT-phase seems to accelerate over the whole film thickness. At approximately 8 nm this intensity overtakes the one of the β-phase.

These observations indicate that close to the substrate, i.e., in the first 2−3 monolayers, 6T seems to arrange preferably in the β-phase. With increasing substrate temperature (from 303 to 373 K) the thermal energy of the molecules is enhanced. Therefore, it is more likely for the molecules to arrange in a thermodynamically favorable configuration. This results in the formation of larger crystal domains of the LT-phase. However, still some β-domains are formed at a substrate temperature of 373 K, presumably due to a templating effect of the β-domains formed in the first few monolayers. This is schematically indicated in Figure 6c.

After approximately 7 nm the film growth seems to be mostly decoupled from the substrate interaction. Above this thickness the diffusion of the molecules is dominated by the intermolecular interaction.

Overall, the results appear to be a rather typical case of competition of phases similar in energy in small molecule OSCs. However, due to the subtleties in the energy landscape, each system has to be studied individually. Nevertheless, for different organic semiconductors similar effects have been reported. For instance, pentacene exhibits two different phases in thin film growth, depending *inter alia* on the substrate temperature,[56] similar to the results reported in this paper. A substrate induced layer is mainly formed up to a critical thickness, and above this the film predominately grows in the bulk crystal phase.[57] For diindenoperylene, low substrate temperatures can lead to the formation of lying domains (λ-orientation) which are energetically unfavorable, but kinetically favored. For the formation of upright standing domains (σ-orientation), which have a lower total surface energy, a potential barrier needs to be overcome by the thermal energy of molecules. This is only achieved at higher substrate temperatures.[39,58] We find a similar behavior for 6T (Figure 4), indicating that this might be a general effect for rodlike oligomers.[6,7] These different phases affect strongly the usually anisotropic optical properties in OSCs.[11,59] Also, the electrical transport is affected, in particular, by phase boundaries.[60]

CONCLUSION

In conclusion, we used X-ray scattering experiments to identify and study the competing interactions of different crystal phases in the thin film growth of α-sexithiophene. We found that the substrate temperature has an important influence on the formation of the different phases. By comparing our findings with the results reported by Moser et al.,[19] we find that the effect of decreasing the substrate temperature is similar to increasing the rate of deposition of the molecule, and one obtains at least qualitatively similar films. Increasing the substrate temperature from 233 to 373 K leads also to an increase of the in-plane coherent crystallite size by a factor of 2, for both crystal phases. From real-time GIXD data we deduce that the β-phase is induced by the substrate and only prominent during the early phase of growth. For the film grown at a substrate temperature of 373 K, we find a critical thickness of approximately 8 nm beyond which the LT-phase dominates the growth of the film. We conclude that the initial phase of the growth is dominated by the influence of the substrate, and after a certain temperature-dependent thickness the growth is more or less decoupled from the substrate and dominated by temperature effects. Still templating effects of the initial crystal phase are relevant and lead to the formation of further β-phase domains.

DOI: 10.1021/jp510321k
J. Phys. Chem. C 2015, 119, 819−825

AUTHOR INFORMATION

Corresponding Author

*E-mail: frank.schreiber@uni-tuebingen.de (F.S.).

Notes

The authors declare no competing financial interest.

ACKNOWLEDGMENTS

We gratefully acknowledge the MS-X04SA/Surface Diffraction beamline staff for their assistance during experiments at the Swiss Light Source. This work was supported by the German Research Foundation (DFG) within the priority program SPP 1355 "Elementary Processes of Organic Solar Cells" and by the Baden-Württemberg Stiftung. C.L. thanks the Carl-Zeiss-Stiftung for funding, and R.B. acknowledges funding by HYMEC.

REFERENCES

(1) *Physics of Organic Semiconductors*, 2nd ed.; Brütting, W., Adachi, C., Ed.; Wiley VCH-Verlag: Weinheim, 2012.

(2) Forrest, S. R. The path to ubiquitous and low-cost organic electronic appliances on plastic. *Nature* **2004**, *428*, 911−918.

(3) Bernède, J. C. Organic photovoltaic cells: History, principle and techniques. *J. Chil. Chem. Soc.* **2008**, *53*, 1549−1564.

(4) Kelley, T. W.; Baude, P. F.; Gerlach, C.; Ender, D. E.; Muyres, D.; Haase, M. A.; Vogel, D. E.; Theiss, S. D. Recent progress in organic electronics: Materials, devices, and processes. *Chem. Mater.* **2004**, *16*, 4413−4422.

(5) Farchioni, R.; Grosso, G. *Organic Electronic Materials*; Springer-Verlag: Berlin, 2001.

(6) Schreiber, F. Organic molecular beam deposition: Growth studies beyond the first monolayer. *Phys. Status Solidi A* **2004**, *201*, 1037−1054.

(7) Witte, G.; Wöll, C. Growth of aromatic molecules on solid substrates for applications in organic electronics. *J. Mater. Res.* **2004**, *19*, 1889−1916.

(8) Hörmann, U.; Wagner, J.; Gruber, M.; Opitz, A.; Brütting, W. Approaching the ultimate open circuit voltage in thiophene based single junction solar cells by applying diindenoperylene as acceptor. *Phys. Status Solidi RRL* **2011**, *5*, 241−243.

(9) Dinelli, F.; Murgia, M.; Levy, P.; Cavallini, M.; Biscarini, F.; de Leeuw, D. M. Spatially correlated charge transport in organic thin film transistors. *Phys. Rev. Lett.* **2004**, *92*, 116802 (1−4).

(10) Tripathi, A. K.; Pflaum, J. Correlation between ambipolar transport and structural phase transition in diindenoperylene single crystals. *Appl. Phys. Lett.* **2006**, *89*, 082103 (1−3).

(11) Alonso, M. I.; Garriga, M.; Karl, N.; Ossó, J. O.; Schreiber, F. Anisotropic optical properties of single crystalline PTCDA studied by spectroscopic ellipsometry. *Org. Electron.* **2002**, *3*, 23−31.

(12) Heinemeyer, U.; Scholz, R.; Gisslén, L.; Alonso, M. I.; Ossó, J. O.; Garriga, M.; Hinderhofer, A.; Kytka, M.; Kowarik, S.; Gerlach, A.; et al. Exciton-phonon coupling in diindenoperylene thin films. *Phys. Rev. B* **2008**, *78*, 085210 (1−10).

(13) Siegrist, T.; Fleming, R.; Haddon, R.; Laudise, R.; Lovinger, A.; Katz, H.; Bridenbaugh, P.; Davis, D. The crystal structure of the high-temperature polymorph of α-hexathienyl (α-6T/HT). *J. Mater. Res.* **1995**, *10*, 2170−2173.

(14) Servet, B.; Ries, S.; Trotel, M.; Alnot, P.; Horowitz, G.; Garnier, F. X-ray determination of the crystal structure and orientation of vacuum evaporated sexithiophene films. *Adv. Mater.* **1993**, *5*, 461−464.

(15) Servet, B.; Horowitz, G.; Ries, S.; Lagorsse, O.; Alnot, P.; Yassar, A.; Deloffre, F.; Srivastava, P.; Hajlaoui, R. Polymorphism and charge transport in vacuum-evaporated sexithiophene films. *Chem. Mater.* **1994**, *6*, 1809−1815.

(16) Horowitz, G.; Bachet, B.; Yassar, A.; Lang, P.; Demanze, F.; Fave, J.-L.; Garnier, F. Growth and characterization of sexithiophene single crystals. *Chem. Mater.* **1995**, *7*, 1337−1341.

(17) Lang, P.; Ardhaoui, M. E.; Wittmann, J.; Dallas, J.; Horowitz, G.; Lotz, B.; Garnier, F.; Straupe, C. Substrate dependent orientation and structure of sexithiophene thin films. *Synth. Met.* **1997**, *84*, 605−606.

(18) Loi, M. A.; Como, E. D.; Dinelli, F.; Murgia, M.; Zamboni, R.; Biscarini, F.; Muccini, M. Supramolecular organization in ultra-thin films of α-sexithiophene on silicon dioxide. *Nat. Mater.* **2005**, *4*, 81−85.

(19) Moser, A.; Salzmann, I.; Oehzelt, M.; Neuhold, A.; Flesch, H.-G.; Ivanco, J.; Pop, S.; Toader, T.; Zahn, D. R.; Smilgies, D.-M.; et al. A disordered layered phase in thin films of sexithiophene. *Chem. Phys. Lett.* **2013**, *574*, 51−55.

(20) Ivanco, J.; Krenn, J. R.; Ramsey, M. G.; Netzer, F. P.; Haber, T.; Resel, R.; Haase, A.; Stadlober, B.; Jakopic, G. Sexithiophene films on clean and oxidized Si(111) surfaces: Growth and electronic structure. *J. Appl. Phys.* **2004**, *96*, 2716−2724.

(21) Garcia, R.; Tello, M.; Moulin, J. F.; Biscarini, F. Size and shape controlled growth of molecular nanostructures on silicon oxide templates. *Nano Lett.* **2004**, *4*, 1115−1119.

(22) Oelkrug, D.; Egelhaaf, H.-J.; Haiber, J. Electronic spectra of self-organized oligothiophene films with "standing" and "lying" molecular units. *Thin Solid Films* **1996**, *284−285*, 267−270.

(23) Ivanco, J.; Haber, T.; Krenn, J.; Netzer, F.; Resel, R.; Ramsey, M. Sexithiophene films on ordered and disordered TiO_2(110) surfaces: Electronic, structural and morphological properties. *Surf. Sci.* **2007**, *601*, 178−187.

(24) Haber, T.; Ivanco, J.; Ramsey, M.; Resel, R. Epitaxial growth of sexithiophene on TiO_2 (110). *J. Cryst. Growth* **2008**, *310*, 101−109.

(25) Ardhaoui, M.; Lang, P.; Wittmann, J.; Lotz, B.; Garnier, F. Structure organization of sexithiophene vapour deposited onto HOPG and SiH/Si(111). *Synth. Met.* **1999**, *101*, 526−527.

(26) Biscarini, F.; Zamboni, R.; Samorí, P.; Ostoja, P.; Taliani, C. Growth of conjugated oligomer thin films studied by atomic-force microscopy. *Phys. Rev. B* **1995**, *52*, 14868−14877.

(27) Muccini, M.; Murgia, M.; Biscarini, F. Morphology controlled energy transfer in conjugated molecular thin films. *Adv. Mater.* **2001**, *13*, 355−358.

(28) Simbrunner, C.; Hernandez-Sosa, G.; Oehzelt, M.; Djuric, T.; Salzmann, I.; Brinkmann, M.; Schwabegger, G.; Watzinger, I.; Sitter, H.; Resel, R. Epitaxial growth of sexithiophene on mica surfaces. *Phys. Rev. B* **2011**, *83*, 115443 (1−8).

(29) Schwabegger, G.; Djuric, T.; Sitter, H.; Resel, R.; Simbrunner, C. Morphological and structural investigation of sexithiophene growth on KCl (100). *Cryst. Growth Des.* **2013**, *13*, 536−542.

(30) Oehzelt, M.; Berkebile, S.; Koller, G.; Ivanco, J.; Surnev, S.; Ramsey, M. α-sexithiophene on Cu(1 1 0) and Cu(1 1 0)-(2 × 1)O: An STM and NEXAFS study. *Surf. Sci.* **2009**, *603*, 412−418.

(31) Koini, M.; Haber, T.; Berkebile, S.; Koller, G.; Ramsey, M.; Resel, R.; Oehzelt, M. Growth of sexithiophene crystals on Cu(110) and Cu(110)-(2 × 1)O stripe phase - The influence of surface corrugation. *J. Cryst. Growth* **2009**, *311*, 1364−1369.

(32) Prato, S.; Floreano, L.; Cvetko, D.; De Renzi, V.; Morgante, A.; Modesti, S.; Biscarini, F.; Zamboni, R.; Taliani, C. Anisotropic ordered planar growth of α-sexithienyl thin films. *J. Phys. Chem. B* **1999**, *103*, 7788−7795.

(33) Kiguchi, M.; Yoshikawa, G.; Saiki, K. Temperature and thickness dependence of molecular orientation of α-sexithienyl on Cu(111). *J. Appl. Phys.* **2003**, *94*, 4866−4870.

(34) Kiguchi, M.; Yoshikawa, G.; Ikeda, S.; Saiki, K. Molecular orientation control of sexithienyl thin film on Cu substrates. *Surf. Sci.* **2004**, *566−568*, 603−607.

(35) Yoshikawa, G.; Kiguchi, M.; Ikeda, S.; Saiki, K. Molecular orientations and adsorption structures of α-sexithienyl thin films grown on Ag(110) and Ag(111) surfaces. *Surf. Sci.* **2004**, *559*, 77−84.

(36) Oehzelt, M.; Koller, G.; Ivanco, J.; Berkebile, S.; Haber, T.; Resel, R.; Netzer, F. P.; Ramsey, M. G. Organic heteroepitaxy: p-sexiphenyl on uniaxially oriented α-sexithiophene. *Adv. Mater.* **2006**, *18*, 2466−2470.

DOI: 10.1021/jp510321k
J. Phys. Chem. C 2015, 119, 819−825

(37) Koller, G.; Berkebile, S.; Krenn, J. R.; Netzer, F. P.; Oehzelt, M.; Haber, T.; Resel, R.; Ramsey, M. G. Heteroepitaxy of organic-organic nanostructures. *Nano Lett.* **2006**, *6*, 1207−1212.
(38) Djuric, T.; Hernandez-Sosa, G.; Schwabegger, G.; Koini, M.; Hesser, G.; Arndt, M.; Brinkmann, M.; Sitter, H.; Simbrunner, C.; Resel, R. Alternately deposited heterostructures of α-sexithiophene-*para*-hexaphenyl on muscovite mica(001) surfaces: crystallographic structure and morphology. *J. Mater. Chem.* **2012**, *22*, 15316−15325.
(39) Kowarik, S.; Gerlach, A.; Sellner, S.; Schreiber, F.; Cavalcanti, L.; Konovalov, O. Real-time observation of structural and orientational transitions during growth of organic thin films. *Phys. Rev. Lett.* **2006**, *96*, 125504 (1−4).
(40) Krause, B.; Schreiber, F.; Dosch, H.; Pimpinelli, A.; Seeck, O. H. Temperature dependence of the 2D-3D transition in the growth of PTCDA on Ag(111): A real-time x-ray and kinetic Monte Carlo study. *Europhys. Lett.* **2004**, *65*, 372−378.
(41) Heinemeyer, U.; Broch, K.; Hinderhofer, A.; Kytka, M.; Scholz, R.; Gerlach, A.; Schreiber, F. Real-time changes in the optical spectrum of organic semiconducting films and their thickness regimes during growth. *Phys. Rev. Lett.* **2010**, *104*, 257401(1−4).
(42) Frank, C.; Novák, J.; Banerjee, R.; Gerlach, A.; Schreiber, F.; Vorobiev, A.; Kowarik, S. Island size evolution and molecular diffusion during growth of organic thin films followed by time-resolved specular and off-specular scattering. *Phys. Rev. B* **2014**, *90*, 045410 (1−6).
(43) Ritley, K. A.; Krause, B.; Schreiber, F.; Dosch, H. A portable ultrahigh vacuum organic molecular beam deposition system for *in situ* x-ray diffraction measurements. *Rev. Sci. Instrum.* **2001**, *72*, 1453−1457.
(44) Willmott, P. R.; Meister, D.; Leake, S. J.; Lange, M.; Bergamaschi, A.; Böge, M.; Calvi, M.; Cancellieri, C.; Casati, N.; Cervellino, A.; et al. The materials science beamline upgrade at the Swiss light source. *J. Synchrotron Radiat.* **2013**, *20*, 667−682.
(45) Als-Nielsen, J.; McMorrow, D. *Elements of Modern X-ray Physics*, 2nd ed.; John Wiley & Sons, Ltd.: Chichester, 2011.
(46) Parratt, L. G. Surface studies of solids by total reflection of x-rays. *Phys. Rev.* **1954**, *95*, 359−369.
(47) Björck, M.; Andersson, G. GenX: an extensible x-ray reflectivity refinement program utilizing differential evolution. *J. Appl. Crystallogr.* **2007**, *40*, 1174−1178.
(48) Farahzadi, A.; Niyamakom, P.; Beigmohamadi, M.; Meyer, N.; Keiper, D.; Heuken, M.; Ghasemi, F.; Tabar, M. R. R.; Michely, T.; Wuttig, M. Stochastic analysis on temperature-dependent roughening of amorphous organic films. *Europhys. Lett.* **2010**, *90*, 10008 (1−5).
(49) Dürr, A. C.; Schreiber, F.; Münch, M.; Karl, N.; Krause, B.; Kruppa, V.; Dosch, H. High structural order in thin films of the organic semiconductor diindenoperylene. *Appl. Phys. Lett.* **2002**, *81*, 2276−2278.
(50) Hinderhofer, A.; Schreiber, F. Organic-organic heterostructures: Concepts and applications. *ChemPhysChem* **2012**, *13*, 628−643.
(51) Scherrer, P. Bestimmung der Größe und der inneren Struktur von Kolloidteilchen mittels Röntgenstrahlen. *Nachr. Ges. Wiss. Göttingen, Math-Phys. Kl.* **1918**, *1918*, 98−100.
(52) Kowarik, S.; Gerlach, A.; Sellner, S.; Cavalcanti, L.; Schreiber, F. Dewetting in an organic semiconductor thin film observed in real-time. *Adv. Eng. Mater.* **2009**, *11*, 291−294.
(53) Hinderhofer, A.; Gerlach, A.; Kowarik, S.; Zontone, F.; Krug, J.; Schreiber, F. Smoothing and coherent structure formation in organic-organic heterostructure growth. *Eur. Phys. Lett.* **2010**, *91*, 56002 (1−5).
(54) Kowarik, S.; Gerlach, A.; Schreiber, F. Organic molecular beam deposition: Fundamentals, growth dynamics, and *in-situ* studies. *J. Phys.: Condens. Matter* **2008**, *20*, 184005 (1−12).
(55) Banerjee, R.; Novák, J.; Frank, C.; Lorch, C.; Hinderhofer, A.; Gerlach, A.; Schreiber, F. Evidence for kinetically limited thickness dependent phase separation in organic thin film blends. *Phys. Rev. Lett.* **2013**, *110*, 185506 (1−5).
(56) Dimitrakopoulos, C. D.; Brown, A. R.; Pomp, A. Molecular beam deposited thin films of pentacene for organic field effect transistor applications. *J. Appl. Phys.* **1996**, *80*, 2501−2508.
(57) Bouchoms, I.; Schoonveld, W.; Vrijmoeth, J.; Klapwijk, T. Morphology identification of the thin film phases of vacuum evaporated pentacene on SiO_2 substrates. *Synth. Met.* **1999**, *104*, 175−178.
(58) Dürr, A. C.; Koch, N.; Kelsch, M.; Rühm, A.; Ghijsen, J.; Johnson, R. L.; Pireaux, J.-J.; Schwartz, J.; Schreiber, F.; Dosch, H.; et al. Interplay between morphology, structure, and electronic properties at diindenoperylene-gold interfaces. *Phys. Rev. B* **2003**, *68*, 115428 (1−12).
(59) Hinderhofer, A.; Heinemeyer, U.; Gerlach, A.; Kowarik, S.; Jacobs, R. M. J.; Sakamoto, Y.; Suzuki, T.; Schreiber, F. Optical properties of pentacene and perfluoropentacene thin films. *J. Chem. Phys.* **2007**, *127*, 194705 (1−6).
(60) Liscio, F.; Albonetti, C.; Broch, K.; Shehu, A.; Quiroga, S. D.; Ferlauto, L.; Frank, C.; Kowarik, S.; Nervo, R.; Gerlach, A.; et al. Molecular reorganization in organic field-effect transistors and its effect on two-dimensional charge transport pathways. *ACS Nano* **2013**, *7*, 1257−1264.

DOI: 10.1021/jp510321k
J. Phys. Chem. C 2015, 119, 819−825